Two-photon polymerization: investigation of chemical and mechanical properties of resins using Raman microspectroscopy

Li Jia Jiang, Yun Shen Zhou, Wei Xiong, Yang Gao, Xi Huang, Lan Jiang, Tommaso Baldacchini, Jean-François Silvain, Yong Feng Lu

Two-photon polymerization: investigation of chemical and mechanical properties of resins using Raman microspectroscopy

Li Jia Jiang,[1] Yun Shen Zhou,[1] Wei Xiong,[1] Yang Gao,[1] Xi Huang,[1] Lan Jiang,[2] Tommaso Baldacchini,[1,3] Jean-Francois Silvain,[4] and Yong Feng Lu[1,*]

[1]*Department of Electrical Engineering, University of Nebraska-Lincoln, Lincoln, Nebraska 68588-0511, USA*

[2]*Department of Mechanical and Automation Engineering, Beijing Institute of Technology, Beijing 100081, China*

[3]*Technology and Applications Center, Newport Corporation, Irvine, California 92606, USA*

[4]*Université Bordeaux 1, Institut de Chimie de la Matière Condensée de Bordeaux (ICMCB), CNRS, 33608 Pessac, France*

**Corresponding author: ylu2@unl.edu*

Received March 11, 2014; revised April 3, 2014; accepted April 7, 2014;
posted April 11, 2014 (Doc. ID 207930); published May 14, 2014

In this study, the degree of conversion (DC) of an acrylic-based resin (IP-L 780) in two-photon polymerization (TPP) is systematically investigated via Raman microspectroscopy. A quantitative relationship between TPP laser parameters and the DC of the resin is established. Nonlinear increase in DC with increased laser average power is observed. The resin DC is more sensitive to the laser average power than the laser writing speed. Nanoindentation was employed to correlate the results obtained from Raman microspectroscopy with the mechanical properties of microstructures fabricated by TPP. At constant writing speeds, microstructures fabricated with high laser average powers possess high hardness and high reduced Young's modulus (RYM), indicating high DCs. The results are in line with high DCs measured under the same TPP parameters in Raman microspectroscopy. Raman microspectroscopy is proved to be an effective, rapid, and nondestructive method characterizing microstructures fabrication by TPP.

OCIS codes: (350.3390) Laser materials processing; (160.5470) Polymers; (220.4000) Microstructure fabrication; (170.5660) Raman spectroscopy.
http://dx.doi.org/10.1364/OL.39.003034

Over the past decades, two-photon polymerizatioon (TPP) has emerged as a highly promising technique for fabricating three-dimensional (3D) microstructures. It permits the fabricatioon of microstructureswith feature sizes on the order of tens of nanometers and with relatively high throughputs [1,2]. In TPP, a laser beam from a femtosecond (fs) laser is tightly focused in a resin. Due to optical nonlinearity, light absorption is confined within the laser beam focal volume allowing for the realization of true 3D writing. Furthermore, it has been demonstrated that subwavelength feature sizes are achievable [1,3]. Novel fabrication techniques combined with TPP have been also reported to improve the TPP resolution and throughput, such as stimulated emission depletion (STED) fluorescence microscopy [4] and continuous flow lithography [5]. Moreover, in TPP, hybrid polymer composites were applied to achieve the broadening of microstructure functionalities [6,7]. A large variety of applications has been investigated using TPP, such as 3D micro-optics [8], nanophhotonics [9,10], microelectromechanical systems [11], bioengineering [12–15], and microfluidics [16].

In acrylic-based resins, the degree of conversion (DC) is used to quantify the amount of consumed carbon-carbon double bonds (C═C) during polymerization. It is related to the crosslinking of the ultimate polymers [17,18]. In TPP, the DCs of resins can significantly affect the final stability and mechanical properties of the fabricated microstructures [19,20]. Thus, establishing the correlation between the TPP parameters and corresponding DCs is a fundamental step to achieving precise fabrication of desired structures using TPP.

Several methods have been used to extrapolate DC values of polymers: differential scanning calorimetry (DSC); Fourier transform infrared (FTIR) spectroscopy; Raman microspectroscopy; and more recently, coherent anti-Stokes Raman scattering (CARS) spectroscopy [18–24]. At the present time, DSC is the industry-standard for characterizing DCs. Unfortunately, this thermoanalytical technique has a stringent minimum weight requirement and frequently causes damage to the samples [18]. Therefore, it is not suitable for testing microstructures fabricated by TPP. Poor spatial resolution and specific sample preparations are among the drawbacks of FTIR spectroscopy [18,21]. Although unique in its ability to monitor chemical processes in real-time, CARS is not widely available and its signal is often difficult to interpret [22]. Raman microspectroscopy is probably the best choice for the static characterization of microstructures fabricated by TPP. It allows for *in situ* and nondestructive monitoring of specific bond vibrations with superior spectral resolution and minimum sample preparation [18]. Meanwhile, for characterizing microstructures fabricated via TPP, the influences of hatching distances on DCs have been demonstrated using Raman microspectroscopy [20].

In this study, we investigated the DCs of microstructures fabricated with TPP using Raman microspectroscopy and established a quantitative relationship between DC and TPP writing parameters. This relationship has been confirmed and correlated on the basis of mechanical property measurements gathered using nanoindentation.

The photoresist used in this study is IP-L 780 (Nanoscribe GmbH). It consists a branched acrylic monomer

and an α-aminoketone photoinitiator. During polymerization, the C═C bonds of the ester units in the monomer are consumed to form carbon-carbon single bonds (C—C) leading to a highly crosslinked polymer.

TPP microfabrication was performed with a 3D laser lithography system (Nanoscribe GmbH, Photonic Professional). The excitation source is an fs laser with an emission center wavelength, pulse width, and repetition rate of 780 nm, 120 fs, and 100 MHz, respectively. The laser beam was focused within the resin using a 100× microscope objective with a numerical aperture of 1.3. The samples for Raman characterization include a series of solid cubes with dimensions of 10 μm × 10 μm × 8 μm fabricated using different TPP parameters. For nanoindentation characterization, solid cubes with dimensions of 20 μm × 20 μm × 4 μm were fabricated. All the microstructures were fabricated with 200 nm hatching distance.

Raman spectra were recorded using a Renishaw Raman microscope (inVia H 18415). The excitation source is a diode laser with a wavelength of 785 nm. Excitation and signal collection were carried out using a 100× objective with a numerical aperture of 0.85. The laser average power was 10 mW. Raman spectra were recorded with an accumulation time of 10 s.

Nanoindentation tests were performed using a Hysitron TI 750 Ubi nanoindenter. A conical-shaped probe (TI-0093) with a tip radius of 3 μm was used to minimize plastic deformation and stress concentrations [25]. Loading distances were fixed at 500 nm. Working times were 10 s for the loading and unloading processes, and 3 s for the creep processes.

Representative Raman spectra of nonpolymerized and polymerized IP-L 780 are shown in Fig. 1. Two distinctive peaks are observed at 1635 and 1723 cm^{-1}, and are ascribed to the vibrational modes of the C═C and the carbonyl (C═O) groups of the monomer units, respectively [22]. Upon polymerization, the C═C bonds are homolytically opened and converted to C—C bonds. Therefore, as a consequence of the diminished concentration of the C═C bonds, the intensity of the peak at 1635 cm^{-1} reduces during polymerization. The Raman peak at 1723 cm^{-1} is utilized as an internal reference when calculating polymer DCs since the peak of C═O bonds does not change upon polymerization [22].

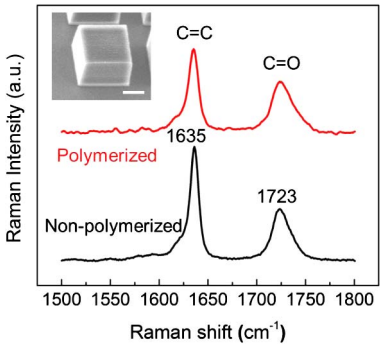

Fig. 1. Raman spectra of polymerized and nonpolymerized IP-L 780. The spectra are shifted vertically for viewing clarity. The inset shows a typical scanning electron micrograph of a solid cube (5 μm scale bar).

To understand how the writing parameters in TPP affect the DC of polymerized IP-L 780, Eq. (1) is used to extrapolate DC values from Raman spectra [22]. $A_{C=C}$, $A_{C=O}$, $A'_{C=C}$ and $A'_{C=O}$ are the integrated peak intensities of Raman peaks related to the C═C and C═O moieties in the polymerized and the nonpolymerized resins, respectively.

$$\mathrm{DC} = \left[1 - \left(\frac{A_{C=C}/A_{C=0}}{A'_{C=C}/A'_{C=0}}\right)\right] \times 100. \quad (1)$$

A comprehensive representation of how average laser powers and writing speeds affect the DCs of IP-L 780 is shown in Fig. 2. At constant writing speeds, DC values monotonically increase with increasing laser powers. At a writing speed of 20 μm/s, a nonlinear increase in DC from 26% to 42% is observed with the increasing laser power. The maximum laser power used is 15 mW; above that the resin begins to boil and bubble, and therefore cannot form stable microstructures. The resin boiling and bubbling are ascribed to the significant temperature changes in overexposure regimes [26]. Below the critical laser power, the temperature within the resin does not change obviously [26]. The maximum DC is ascribed to the branched nature of the acrylic monomer. During polymerization, crosslinked oligomers are formed that are difficult to diffuse freely. With increasing DCs, the mobility of the oligomers is so limited that further polymerization process is terminated, therefore limiting the maximum DC to below 50% [22]. The phenomenon of incomplete conversion of a resin into a polymer is common when using highly branched acrylic monomers. Similar results are observed to be independent of the polymerization initiation mechanism [27]. To verify the maximum DC value obtained in the TPP process, IP-L 780 was polymerized using a conventional UV light source (395 nm, 12 mW/cm^2). The maximum DC value of 45% was obtained via the conventional photopolymerization process, which coincides well with the maximum DC value obtained by TPP.

It is interesting to find out that DC values are more sensitive to average laser power than writing speed. Depending on the writing speeds from 80 to 20 μm/s, maximum DC values range from 35% to 42%. A two-fold increase is observed in the measured DCs when increasing the average laser powers from 8 to 15 mW. At constant average

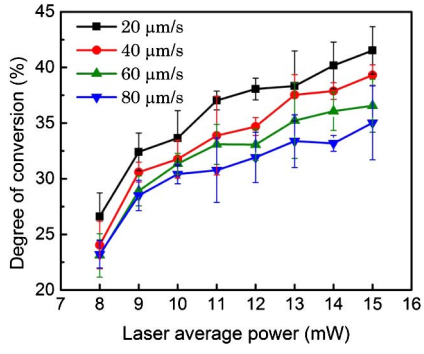

Fig. 2. Dependence of polymerized IP-L 780 DC on average laser power and writing speed.

Table 1. DC Comparison of Data Points

Point	Writing Speed (μm/s)	Average Laser Power (mW)	Q	DC (%)
A	60	10	1.67	31.34
B	80	12	1.80	31.91
C	60	13	2.82	35.23
D	80	15	2.81	35.03
E	60	14	3.27	36.01
F	20	8	3.20	26.61

laser powers, DC values monotonically increase with decreasing writing speeds. Increases of about 5 to 6 percentage points are observed by decreasing the writing speed from 80 to 20 μm/s. It indicates that the concentration of radicals generated by two-photon absorption is more sensitive to the average laser power than writing speed, similar to the reported results [28].

Based on the two-photon absorption model [1], it is expected that the DC would be proportional to the square of average laser power and the reciprocal of writing speed. Therefore, it is predicted that TPP parameter sets with a similar Q index (average laser power)^2/writing speed) would lead to a similar DC. It is found that, as shown in Table 1, the results obtained at high writing speeds fit well with the above prediction, indicating that both average laser power and writing speed play an important role in determining the DC value in high writing speed regions (i.e., 60 and 80 μm/s). For example, A and B as listed in Table 1 have similar DC values (31.34% and 31.91%, respectively) but fabricated using different parameters. The same phenomena can be found in C and D as well. However, the results obtained at low writing speed do not fit with the above prediction very well. For example, although the data point F has a similar Q index (~3.2) as the data point E, the DC value (26.61%) of F is much lower than the DC value (36.01%) of E. The results suggest that in the low writing speed region the average laser power plays a more important role than the writing speed in determining the DC value. In other words, the average laser power dominantly controls the DC value in the low writing speed region. It is believed that, for a given average laser power, the DC increases rapidly at the early stage of TPP exposure and gradually becomes saturated at the late stage of TPP exposure [29]. Therefore, the DC values of data points in the low writing speed region (i.e., 20 μm/s) no longer follow the same reciprocal relationship with writing speed as that in the high writing speed region (i.e., 60 and 80 μm/s). It is expected that DC values in higher writing speed region (>80 μm/s) will match with the theoretical prediction of the DC dependence on squared average laser power much better than that in the low writing speed region.

By using Raman imaging, spatial distribution of the DC values of the polymerized resins is visualized in Fig. 3. Figures 3(a)–3(d) exhibit top-surfaces of four solid cubes fabricated by TPP at a constant writing speed of 20 μm/s and average laser powers of 8, 10, 12, and 14 mW, respectively. For each pixel (1 × 1 μm) in Fig. 3, a Raman spectrum of the sample is acquired, and a value of DC is assigned to that pixel using Eq. (1). The false-color contrast represents DC variation in the sample. As the

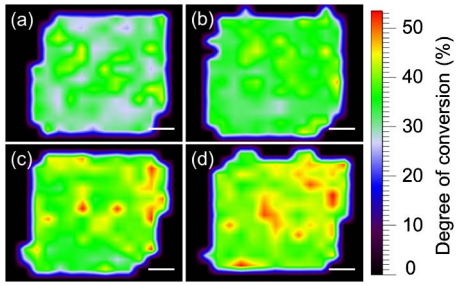

Fig. 3. Raman mapping of DCs under average laser powers of 8, 10, 12, and 14 mW, respectively, from (a) to (d), with a constant writing speed of 20 μm/s. The scale bars are 2 μm.

average laser power increases, the overall intensity of the extrapolated DC signals from the sample increases as well. Some inhomogeneous spots were observed in Raman mapping. There are two reasons for the inhomogeneity. One is ascribed to the signal acquisition process. It is believed that the focal position of the Raman laser may not always be perfectly on the sample surface in Z direction, which may mainly cause the relatively large inhomogeneity in the Raman mapping images. Besides, the instability of laser power during the long-time Raman mapping process (5–6 h) may also induce the additional inhomogeneity. The other reason is ascribed to the inhomogeneity of as-fabricated samples by the TPP process. The TPP parameters may not be well optimized to achieve high uniformity of the polymerized samples. From the TPP fabrication aspect, optimizing the degree of voxels overlapping [30,31] and TPP parameters will further improve the uniformity. The results show that Raman mapping provides a direct visualization on DCs of polymerized resin with different TPP parameters.

The mechanical properties of polymers are significantly influenced by DCs [19]. Generally speaking, a high DC results in improved mechanical properties [27]. Thus, the nanoindentation technique was used to verify the effectiveness of Raman microspectroscopy in evaluating DCs. Based on the load-displacement curve, the hardness H and reduced Young's modulus (RYM) E_r can be determined using Eq. (2):

$$H = \frac{P_{\max}}{A} \quad \text{and} \quad E_r = \frac{dP}{dh}\frac{\sqrt{\pi}}{2\sqrt{A}}, \tag{2}$$

where A is the projected contact area, $P_{\max}$ is the maximum load and h is the displacement of indenter relative to the specimen. The relationship between E_r and Young's Modulus E is given by Eq. (3):

$$\frac{1}{E_r} = \frac{(1-\nu)}{E} + \frac{(1-\nu_i^2)}{E_i}, \tag{3}$$

where ν is the Poisson ratio of the resin sample, ν_i and E_i are the parameters for the indenter, which are 0.07 and 1140 GPa, respectively. Most materials have Poisson's ratio values ranging from 0.0 to 0.5, which represent the negative ratio of transverse to axial strain [32]. The E_r describes the contact between a microstructure and the nanoindenter tip, and represents the elastic deformation that occurs in microstructures as shown

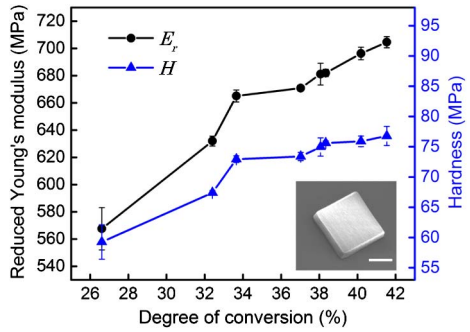

Fig. 4. RYM and hardness of TPP polymerized structures as the functions of the DCs. As-fabricated cubic structures are shown at the lower-right inset with 10 μm scale bar.

in Eq. (2). If the crosslink density changes the amount of viscous deformation, the Poisson's ratio of the as-fabricated structures will change, too. Since Young's modulus highly depends on Poisson's ratio, as shown in Eq. (3), there could be a different reaction of polymer against the indentation, which, in turn, affects the modulus calculation [25]. For the convenience of discussion, E_r is discussed in this study to represent the mechanical modulus of the polymerized resin.

Figure 4 shows the variation of E_r and H of polymerized resins with respect to corresponding DCs. It is observed that both E_r and H increase with increasing DCs. The nanoindentation results coincide with the Raman microspectroscopic studies and prove the reliability of Raman microspectroscopy in characterizing the DCs of polymerized structures in TPP. Meanwhile, it quantitatively correlates DCs with the mechanical properties of the polymerized resins.

In conclusion, the dependence of DC on TPP parameters was successfully established by Raman microspectroscopy using the peak intensity change of C═C bonds in resin. DC shows more dependence on the average laser power than the writing speed. Furthermore, DC visualization of the polymerized resin was realized by Raman mapping. The effectiveness of Raman microspectroscopy was also confirmed via nanoindentation measurement, which presents an effective evaluation of mechanical properties on DC variation. The results indicate that Raman microspectroscopy is a convenient and accurate method to characterize TPP processes in molecular levels. Meanwhile, the results reveal how the TPP parameters affect the DCs and how to tailor the future fabrication with effective writing strategy. It is also demonstrated that the Raman microspectroscopy could be used to predict mechanical properties of the fabricated microstructures.

This research work was financially supported by National Science Foundation (CMMI 0900419).

References

1. S. Maruo and J. T. Fourkas, Laser Photon. Rev. **2**, 100 (2008).
2. K. S. Lee, D. Y. Yang, S. H. Park, and R. H. Kim, Polym. Adv. Technol. **17**, 72 (2006).
3. J. Fishcher, G. von Freymann, and M. Wegener, Adv. Mater. **22**, 3578 (2010).
4. L. Li, R. R. Gattass, E. Gershgoren, H. Hwang, and J. T. Fourkas, Science **324**, 910 (2009).
5. S. C. Laza, M. Polo, A. A. R. Neves, R. Cingolani, A. Camposeo, and D. Pisignano, Adv. Mater. **24**, 1304 (2012).
6. K. Kurselis, R. Kiyan, V. N. Bagratashvili, V. K. Popov, and B. N. Chichkov, Opt. Express **21**, 31029 (2013).
7. S. Ushiba, S. Shoji, K. Masui, P. Kuray, J. Kono, and S. Kawata, Carbon **59**, 283 (2013).
8. M. Malinauskas, H. Gilbergs, A. Zukauskas, V. Purlys, D. Paipulas, and R. Gadonas, J. Opt. **12**, 035204 (2010).
9. G. von Freymann, A. Ledermann, M. Thiel, I. Staude, S. Essig, K. Busch, and M. Wegener, Adv. Funct. Mater. **20**, 1038 (2010).
10. M. Thiel, G. V. Freymann, and M. Wegener, Opt. Lett. **32**, 2547 (2007).
11. S. Tottori, L. Zhang, F. Qiu, K. K. Krawczyk, A. Franco-Obregon, and B. J. Neison, Adv. Mater. **24**, 811 (2012).
12. F. Klein, B. Richter, T. Striebel, C. M. Franz, G. V. Freymann, M. Wegener, and M. Bastmeyer, Adv. Mater. **23**, 1341 (2011).
13. F. Klein, T. Striebel, J. Fischer, Z. X. Jiang, C. M. Franz, G. V. Freymann, M. Wegener, and M. Bastmeyer, Adv. Mater. **22**, 868 (2010).
14. A. Koroleva, A. A. Gill, I. Ortega, J. W. Haycock, S. Schile, S. D. Gittard, B. N. Chichkov, and F. Claeyssens, Biofabrication **4**, 025005 (2012).
15. T. Weiß, G. Hildebrand, R. Schade, and K. Liefeith, Eng. Life Sci. **9**, 384 (2009).
16. S. Jariwala, K. Venkatakrishnan, and B. Tan, Opt. Express **18**, 1630 (2010).
17. T. Baldacchini and Z. Ruben, Opt. Express **18**, 19219 (2010).
18. L. E. Silva Soares, A. A. Martin, and A. L. Barbosa Pinheiro, J. Clin. Laser Med. Surg. **21**, 357 (2003).
19. N. Emami and K. J. Söderholm, Open Dentistry J. **3**, 202 (2009).
20. F. Burmeister, S. Steenhusen, R. Houbertz, U. D. Zeitner, S. Nolte, and A. Tunnermann, J. Laser Appl. **24**, 042014 (2012).
21. N. Silikas, G. Eliades, and D. C. Watts, Dental Materials **16**, 292 (2000).
22. T. Baldacchini, M. Zimmerley, C. H. Kuo, E. O. Potma, and R. Zadoyan, J. Phys. Chem. B **113**, 12663 (2009).
23. S. K. H. Khalil, M. A. Allam, and W. A. Tawfik, European J. Dentistry **1**, 72 (2007).
24. W. C. Wu, D. Sbrestba, X. Wei, J. Q. Ling, W. H. Zhang, and J. Chen, J. Endodont. **36**, 329 (2010).
25. K. Cicha, T. Koch, J. Torgersen, Z. Li, R. Liska, and J. Stampfl, J. Appl. Phys. **112**, 094906 (2012).
26. J. B. Mueller, J. Fischer, Y. J. Mange, T. Nann, and M. Wegener, Appl. Phys. Lett. **103**, 123107 (2013).
27. V. M. Urban, A. L. Machado, C. E. Vergani, E. G. Jorge, L. P. S. D. Santos, E. R. Leite, and S. V. Canevarolo, Mater. Res. **10**, 191 (2007).
28. K. Cicha, Z. Li, K. Stadlmann, A. Ovsianikov, R. Markut-Kohl, R. Liska, and J. Stampfl, J. Appl. Phys. **110**, 064911 (2011).
29. H. B. Sun, K. Takada, M. S. Kim, K. S. Lee, and S. Kawata, Appl. Phys. Lett. **83**, 1104 (2003).
30. K. Takada, H. B. Sun, and S. Kawata, Appl. Phys. Lett. **86**, 071122 (2005).
31. R. Guo, S. Xiao, X. Zhai, J. Li, A. Xia, and W. Huang, Opt. Express **14**, 811 (2006).
32. J. M. Gere and B. J. Goodno, *Mechanics of Materials*, 7th ed. (Cengage Learning, 2009).